Current Deflection NDE for the Inspection and Monitoring of Pipes

R. Jarvis[a,*], P. Cawley[a], P. B. Nagy[a,b]

[a] *NDE Group, Mechanical Engineering Department, Imperial College London, London, SW7 2AZ, United Kingdom*
[b] *Department of Aerospace Engineering and Engineering Mechanics, University of Cincinnati, Cincinnati, Ohio 45221, USA*

Abstract

Routine inspection of oil and gas pipes for time dependent degradation is essential. Pipelines are most commonly inspected using In-Line Inspection (ILI), however restrictions from pipe geometry, features or flow rate can prevent its use. Facility pipework rarely facilitates ILI, and external inspection often warrants the undesirable removal of the pipe insulation and cladding. This work investigates the applicability of a current deflection non-destructive evaluation technique for both the detection and growth monitoring of defects, particularly focusing on corrosion. Magnetic sensors are used to monitor variations in the spatial distribution of the induced magnetic flux density outside a pipe that arise from deflection of an injected electric current around inner or outer wall defects. An array of orthogonal magnetoresistive sensors has been used to measure the magnetic flux density surrounding six-inch schedule 40 seamless and welded carbon steel and austenitic steel pipes. The measurements were stable and repeatable to the order of 100 pT which suggests that the defect detection or growth monitoring of corrosion-type defects may be possible with a few amps of injected current when measurements are taken at around 50 mm lift-off. The sensitivity of the technique is dependent on factors including defect geometry, sensor lift-off, bends, variations in nominal pipe geometry or material properties, and the presence of ferromagnetic objects, each of which were investigated using either experiment or a validated finite element model.

Keywords: Current deflection, SHM, Electromagnetic NDE, Pipe NDT

1. Introduction

Oil and gas pipeline failure can have catastrophic consequences. Pipelines are subject to time-dependent degradation, most commonly in the form of corrosion, therefore routine inspection must be completed to identify the potential areas at risk of failure [1]. Internal or In-Line Inspection (ILI) allows long stretches of pipe to be rapidly inspected for damage by using smart pigs, devices that use NDE techniques such as Magnetic Flux Leakage (MFL) or ultrasonic thickness gauging to give a direct indication of the pipe wall condition [2]. Their use is limited, however, to sections of pipe which do not exhibit features such as sharp bends or diameter changes which could cause the device to become stuck [2]. For this reason, in addition to the requirements of a minimum flow rate and launches and traps for the device, many pipes must be inspected with alternative means. Similarly, the inspection and monitoring of facility piping cannot be completed using ILI and often warrants the costly and time-consuming need to remove the cladding and insulation coating before applying external NDE methods.

Eddy Current techniques such as Pulsed Eddy Current (PEC) [3, 4, 5], Gradient PEC [6] and Saturated Low Frequency Eddy Current (SLOFEC) [7, 8] have been proposed for the inspection of inner and outer wall defects in difficult to inspect pipes via external application outside of cladding and insulation. PEC testing is slow, and can only detect generalised wall loss [9]. Gradient-PEC offers greater sensitivity to hidden corrosion, but can overestimate corrosion size leading to false alarms [6]. SLOFEC requires a DC magnetic field to saturate the pipe so that induced eddy currents can penetrate to the inner surface of the material. An increase in lift-off (the distance between the probe and the sample) results in a reduction of the amplitude of the Eddy currents and the magnitude of the DC field present in the sample. For this reason, if a significant lift-off (>10 mm) is to be tolerated, the size and power requirements of the testing equipment quickly becomes very large. Pulsed MFL and Pulsed Magnetic Reluctance (PMR) have been proposed for use together to detect and size sub-surface defects in ferromagnetic material, although further research is required before industrial deployment [10].

Modified ILI pigs with the capability to collapse to multiple diameters and pass through pipelines where traditional ILI is unsuitable have been proposed that use PEC and RFEC [11, 12, 13], however the requirement for launches and traps for the device remains and the risk of becoming stuck is not fully eliminated.

Guided ultrasonic wave methods are well suited to in-

*Corresponding author
Email addresses: r.jarvis13@imperial.ac.uk (R. Jarvis), p.cawley@imperial.ac.uk (P. Cawley), p.nagy@uc.edu (P. B. Nagy)

spection of pipes that do not support ILI, and can detect corrosion removing 5% of the pipe wall thickness over a range of >50 m from the transducer array [14, 15, 16] however, the requirement of good coupling with the pipe means that thick or viscous coatings must be removed at the transduction site. Furthermore, the sensitivity near to pipe features is reduced, and the interpretation of the signal is operator dependent, particularly in complex lines. The test range is also reduced for buried pipes predominantly due to energy leakage into the soil [17]. Permanently installed point ultrasonic thickness measurements can accurately monitor the rate of metal loss [18], yet the measurement is localised to the fixed sensor position which warrants a large number of sensors to predict the pipe condition over a large area on a sampling basis.

Radiography has been successfully applied to the in-service detection of corrosion under insulation in pipelines [19, 20, 21]. Through transmission radiography requires access to both sides of the pipe, and for large diameter pipes, either gamma ray or high energy X-rays must be used in order to propagate over such a large distance between source and receiver [22, 23, 24]. Back-scatter radiography may be used when there is access to only one side of the pipe although the scattered radiation is diffuse (non-imaging) and of a low intensity [22]. The use of radiography also has health and safety implications and rigorous standards must be met before its use is justified [20].

The Metal Magnetic Memory (MMM) method has been applied to the non-contact inspection of pipes by measuring peaks in the gradient of the magnetic leakage field of a pipe that can result from amplification of magnetization at locations of stress concentrators due to the magnetomechanical effect [25]. A manifestation of MMM known as the Magnetic Tomography Method (MTM) claims to be able to detect defects at extreme lift-off of over a metre [26, 27, 28]. The relationship between stress and magnetic field is complex, and Augustyniak and Usarek [29] have shown that it is not possible to retrieve a bidirectional relationship between the magnetic field gradient and the local stress level in the pipe because the magnetic field is a function of several inseparable variables, making a quantitative NDE technique based on the MMM method impossible. The "NoPig" method is an above ground inspection method aimed at identifying corrosion on difficult-to-inspect buried pipelines carrying an injected electric current. This method relies on the fact that the magnetic flux density profile surrounding a pipe with metal loss is frequency dependent due to the electromagnetic skin effect and stray magnetic flux leakage [30]. The minimum detectable defect must have 50% metal loss and no information about the defect morphology can be inferred [31]. The distance between the sensor and the pipe is so large ($\sim$ 1.5 m) that the technique is only sensitive to relatively large defects, and sensitivity can be greatly affected by external influences such as busy roads, stray currents and metal objects in the vicinity of the line [31].

"Magnetic Response Imaging" has been developed to detect and monitor corrosion under insulation by measuring the magnetic response of a pipe as it is excited by an alternating magnetic field which is generated using coils wrapped around the pipe [32]. The technique cannot be applied outside of ferromagnetic cladding, and it is unclear how factors other than metal loss can influence the measured signal.

The Alternating Current Field Method (ACFM) allows non-contact detection and sizing of surface breaking cracks in pipes by inducing a uniform high frequency electric current in the surface of the pipe and measuring current deflection around defects by monitoring changes in the induced magnetic field [33, 34]. The technique can be applied outside of a coating up to 10 mm thick [35], is fast and does not require instrument calibration before use [36]. The key disadvantages are that defect detection is limited to surface breaking cracks due to the frequency of the induced current [35, 33]; geometric variations can lead to false alarms; and the large sensor size can cause limitations to access [36]. Potential Drop (PD) methods are able to successfully monitor crack growth from the change in resistance between two electrodes as the increasing defect size lengthens the path of the current [37]. The Field Signature Method (FSM) is based on potential drop methods, and has been used to monitor internal erosion, corrosion and cracking [38], and more recently the ability to characterise pitting has been improved [39]. Galvanic contact with the conductor is required for both PD and FSM, hence insulation must be removed and the methods are not suitable for scanning.

The inability of ACFM to detect inner surface defects can be alleviated by significantly lowering the injection frequency. If the current were to be directly injected into the pipe, a very low frequency current could be made to flow within the pipe and the insulation coating could remain intact except at occasional galvanic injection points. For the inspection of pipelines in an industrial setting, the injection of the current could be facilitated by galvanic attachment of wires separated by significant ($\sim$1 km) intervals, or using the attachments provided by existing cathodic protection testing posts [40]. For facility pipework, the current should be injected and retrieved around the area of interest.

This paper discusses a current deflection technique, that could be considered a hybrid of the ACFM and PD methods, for the application of the inspection and SHM of pipes. In section 2, the principle of the current deflection method is initially be introduced. The experimental methodology is outlined in section 3. The results are presented in section 4. Initially, experimental measurements of the magnetic flux density are given in subsection 4.1, then studies completed with a validated finite element model follow in subsection 4.2 to predict how the lift-off, defect geometry, presence of pipe bends or nearby ferromagnetic objects affect the sensitivity. Magnetic measurements of current deflection in an austenitic pipe are shown

in subsection 4.3, and measurements of a seamless carbon steel pipe are presented in subsection 4.4. Section 5 discusses the results with reference to the application of the technique to both scanning and SHM and section 6 concludes the paper.

2. Principles of method

As an electric current flows axially along a defect-free pipe it induces an azimuthal magnetic field. Upon the presence of a defect, a deviation in the current direction will occur as the path of least electrical resistance is chosen. The clockwise and counter-clockwise rotations of the current around the defect edges induce radial and axial components of the magnetic field near the defect. A reduction in the volume of conductive material at the defect reduces the amount of current at this point which results in a minimum in the azimuthal magnetic field directly above the defect, and maxima at the defect edges. These effects are demonstrated in Fig. 1 for the geometry of a flat plate with a concave defect. The detection and growth monitoring of defects can therefore be achieved by positioning magnetic sensors near the defect and measuring spatial or temporal changes in the three orthogonal components of the magnetic flux density.

The magnetic signals arising from current deflection are small in comparison to the geomagnetic field; however, by using an alternating rather than direct current, phase sensitive detection becomes possible which can effectively eliminate DC bias, drift and other low-frequency noise sources and greatly improve the sensitivity. The depth of penetration of an alternating current into a conductor is governed by the electromagnetic skin effect,

$$\delta = \frac{1}{\sqrt{\pi f \sigma \mu}} \tag{1}$$

where δ, f, μ, σ are the skin depth, frequency of current, conductivity and magnetic permeability respectively [41]. It is advantageous to have a current flow throughout the entire volume of the conductor so that current deflection can occur from defects located anywhere throughout the pipe wall. In ferromagnetic materials, μ tends to be strongly inhomogeneous so to achieve uniform current distribution a current frequency must be chosen such that δ is much larger than the thickness of the conductor so variations in the magnetic properties of the material do not affect the current distribution and the measured magnetic signals are only due to the geometry of the pipe.

3. Experimental methodology

The magnetic flux density was measured using an array of three orthogonally oriented AFF755B Anisotropic Magnetoresistive (AMR) sensors, selected for their high sensitivity, low cost, low power consumption and small size in comparison to fluxgate sensors [42]. Despite the potential

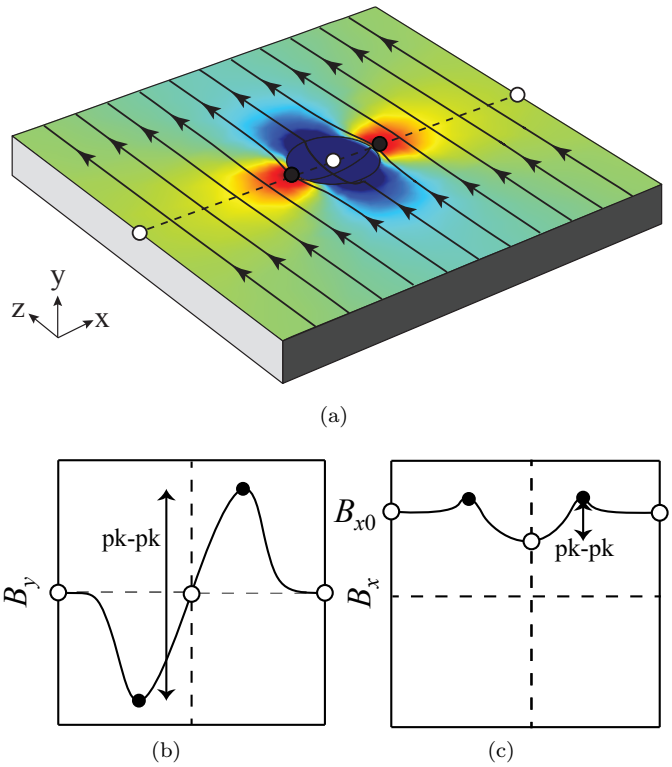

Figure 1: Measurement principle of current field method. (a) Magnitude of the magnetic flux density as a result of current distortion (black arrows) around a concave defect shown in a section of a plate. Profiles of the (b) x and (c) y components of flux density along dashed line in (a). Note the filled circle loci on the graphs that mark the defect edges and the open circles marking the defect center and points far from the defect.

for more highly sensitive sensors based on the giant or tunnelling Magnetoresistive (MR) effects, the AMR selected offered improved stability and low noise (0.19 pT/$\sqrt{\text{Hz}}$). The differential signal from each sensor was read using a SR830 lock-in amplifier using phase sensitive detection. The sensors were multiplexed and read in turn using a LABVIEW interface. The reference signal from the lock-in amplifier allowed a Kepco 36-6D bipolar operational power supply to draw a current of 2 A (RMS) that flowed within the pipe at the frequency of interest. The current injection was achieved via 12 wires evenly spaced around the circumference of the pipe and clamped down onto the metal using a hose grip in order to decrease contact resistance, as shown in the schematic diagram in Fig. 2. Multiple injection points were necessary to allow uniform spread of the injected current over the whole cross section of the relatively short length of pipe. The wires were fed through a slip-ring to ensure that they did not tangle following multiple pipe rotations. Both ends of the pipe were closed with aluminium end caps, and a stainless steel rod was positioned at the pipe centre and held in tension to act as a return path for the current. This was implemented to avoid the need for a long wire for the return current path which would generate a field that could interact with

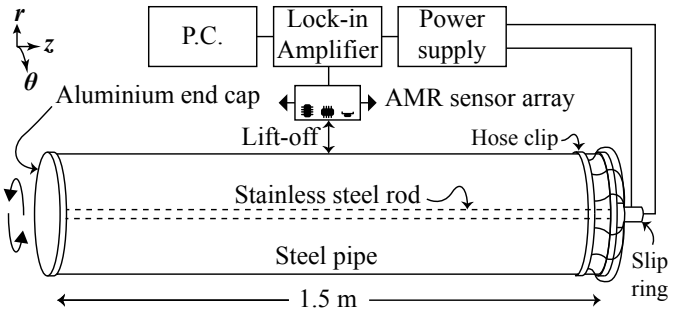

Figure 2: Schematic diagram of pipe scanning rig. Pipe rotation and array position are controlled by stepper motors.

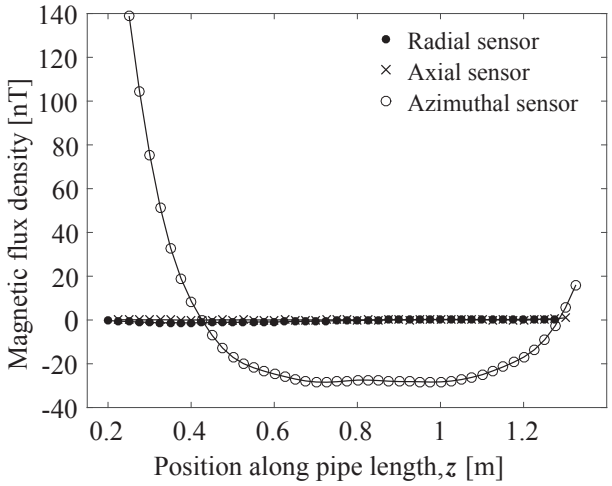

Figure 3: Mean of 15 repeated scans of the magnetic flux density components performed at 10 mm lift-off from a 6" pipe carrying 2 A current at 5 Hz. Pipe ends are located at $z = 0$ m and $z = 1.5$ m. Standard deviations are 282 pT, 198 pT and 205 pT for B_r, B_z, B_θ respectively across the whole scan length.

that from the pipe. The addition of this rod also acted to suppress the otherwise large induced azimuthal component of the magnetic flux density. Before every experiment, a flip-pulse was applied to an integrated set/reset coil inside the sensor chips to ensure the optimization of the sensor performance by reorienting the magnetic domains in the AMR film and correcting for magnetic hysteresis [43].

The position of the sensors relative to the pipe was controlled by a pitch and height adjustable plastic array holder with a sliding mechanism to adjust the lift-off distance. Non-ferromagnetic material was used wherever possible in order to avoid disturbing the induced magnetic field from the injected current.

The sensor array holder was fixed to an aluminium linear actuator which was capable of moving the array along the entire length of the pipe. The rotation of the pipe was facilitated by a worm drive connected to a stepper motor. The acquisition program allowed parameters including the scanning resolution, number of repetitions, inspection frequency and the averaging time to be varied.

1.5 m lengths of 6-inch schedule 40 pipe (wall thickness 7.11 mm, outer diameter 168.4 mm) were selected for testing. Initial experiments were performed on an austenitic steel (grade 302) pipe, and subsequent experiments on a carbon steel pipe. Both longitudinally welded and seamless pipes were tested.

4. Results

4.1. Stability and Repeatability Measurements

In order to assess the suitability of AMR sensors for the measurement of the magnetic flux density signals, the temporal and spatial stability of the measured signal was quantified. Fifteen scans were completed with an overall scan length of 1 m at 10 mm lift-off distance from a longitudinally welded carbon steel pipe with a spatial resolution of 25 mm. The scans were taken on a line diametrically opposite from the longitudinal weld. The pipe carried a 2 A current at 150 mV and 5 Hz. The mean of all fifteen scans is shown in Fig. 3. The standard deviation was calculated to be 282 pT, 198 pT and 205 pT for the radial, axial and azimuthal components respectively across the whole scan length. The radial and axial components stay close to zero along the length of the pipe due to the lack of any defects to perturb the current, with mean values of -400±88 pT and 99±26 pT respectively, where the uncertainty is the standard error of the mean [44]. The azimuthal component exhibits large gradients towards the edges of the pipe due to edge effects and settles to a value of -28 nT towards the centre of the pipe. A misalignment between the axes of the pipe and the rod used for the return current path is likely the reason that the azimuthal component is not reduced to zero away from the pipe ends. The solution to Ampère's law for an infinite cylinder carrying 2 A of current yields a value of the induced magnetic flux density of 22.4 μT in the azimuthal component (the radial and axial components are identically zero), thus the addition of the rod for the return current path has reduced the azimuthal flux density by three orders of magnitude at the pipe centre. This large azimuthal component is largely unimportant as it is the more stable axial and radial components that will be used for defect detection and monitoring, and this method of suppression of the azimuthal component is clearly not possible in the field.

To investigate the temporal stability of the signal, each component of $\bar{B}$ was measured every three minutes over the course of a week with an averaging time of 25 s. A 2 A current was maintained in the pipe and the modulation frequencies chosen were 1 Hz, 5 Hz and 25 Hz. It is important that measurements can be taken at such low frequencies to ensure that the measured magnetic signal is due only to the current distribution as restricted by the pipe geometry and not the electromagnetic skin effect. The results are shown in Fig. 4. As the profiles from all the measurements were similar, only the 5 Hz signal from the radially oriented sensor has been plotted for clarity. The temperature was monitored with a thermocouple.

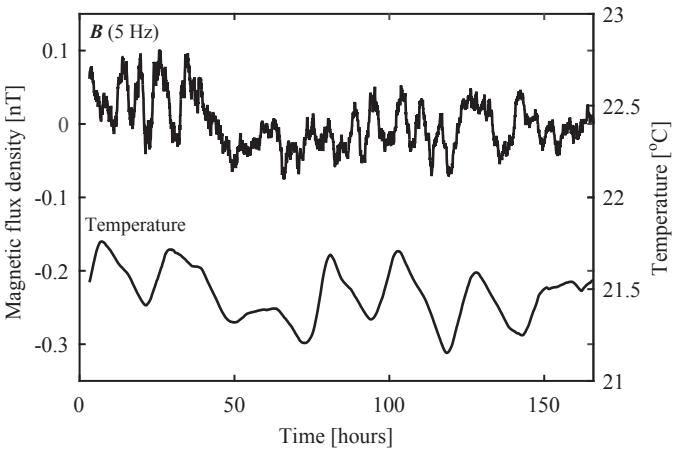

Figure 4: Stability of magnetic signal over a week, measuring B_z halfway along the pipe at 10 mm lift-off with 2 A, 5 Hz current in pipe. Temperature meaured independently using a thermocouple.

There was a small temperature variation of 2°C during the daily cycles. Over the course of the week, a decreasing trend can be noted on both the magnetic flux and temperature measurements. The sensor measurement was not temperature compensated as the range in the magnetic flux density over the entire week was significantly less than 1 nT; however, when utilising AMR sensors in the field where large temperature variations are common, temperature correction is possible through the use of a set/reset coil integrated within the chip. Some additional higher frequency noise is present on the magnetic measurements yet crucially they do not stray far from zero as expected from the measurement of a defect-free pipe. The mean of the radial sensor was -18 ± 550 pT, -80 ± 180 pT and -25 ± 270 at 1 Hz, 5 Hz and 25 Hz respectively where the uncertainty is the standard deviation. The noise density of the sensors was measured as 1.37, 0.46 and 0.32 pT/$\sqrt{\text{Hz}}$ at 1 Hz, 5 Hz and 200 Hz respectively. The chosen inspection frequency should always be far from the mains (line) frequency (50 Hz in Europe or 60 Hz in North America) and its harmonics to avoid electromagnetic interference which reduces the signal to noise ratio.

The lack of any significant drift in the measurement implies that the use of a flip-pulse through the set/reset coil which is sometimes required to reset hysteresis in MR sensors is not a requirement in the lab environment. In further tests it was revealed that the use of the flip-pulse was only necessitated when a strong permanent magnet was brought close to the sensor; the sensors were not saturated by the induced fields from a 2 A current in the lift-off range of interest. In an industrial environment it is likely that a flip-pulse in the set/reset coil would be utilized periodically to reset the magnetic domain orientation in the sensor and to correct for a drifting offset voltage with temperature as variations are likely to be more severe than in the lab.

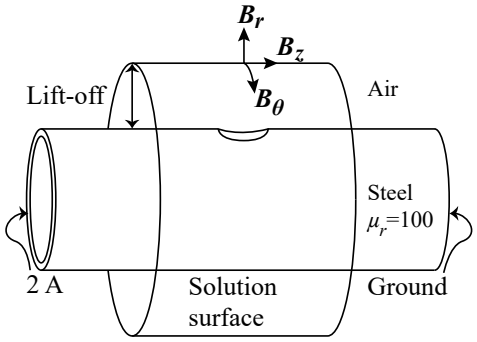

Figure 5: Schematic diagram of FE model with $3T \times 3T$ concave defect in outer surface. The magnetic flux density components computed on the cylindrical surface are shown outside the pipe.

4.2. Finite element simulation

A Finite Element (FE) model has been created using COMSOL Multiphysics® [45] in order to predict the magnetic signals resulting from current deflection. As corrosion is the most common cause of pipeline failure, a concave defect with a diameter three times the wall thickness T, was placed in the outer wall of a six inch schedule 40 steel pipe. The model geometry parameters are shown in Table 1. The radial, axial and azimuthal components of the magnetic flux density were predicted on a cylindrical surface coaxial with the pipe with a radius equal to the pipe outer radius plus the lift-off of interest, as shown in Fig. 5.

Table 1: Values of parameters used in FE model.

Parameter	**Value**	**Unit**
Outer diameter	315.6	mm
Wall thickness	7.1	mm
Concave defect diameter	21.3	mm
Concave defect depth	2.37	mm
Electrical conductivity	4.032×10^6	S/m
Relative magnetic permeability	100	–

4.2.1. Lift-off study

The peak-to-peak values of the perturbations in the magnetic flux density due to the deflection of a 2 A current flowing through the pipe were predicted on this surface as the lift-off distance between the solution surface and the pipe was increased. The results are shown in Fig. 6. The peak-to-peak magnetic flux density has been plotted on a decibel scale normalized to the values at the pipe surface. The FE simulations were run in quasi-DC mode by finding the stationary solutions of Maxwell's equations. For the pipe geometry modelled, this assumption is valid provided the inspection frequency is lower than 12 Hz in carbon steel and 3.5 kHz in non-magnetic austenitic steel so that the current distribution is only affected by the geometry of the conductor and not limited by the electromagnetic skin effect.

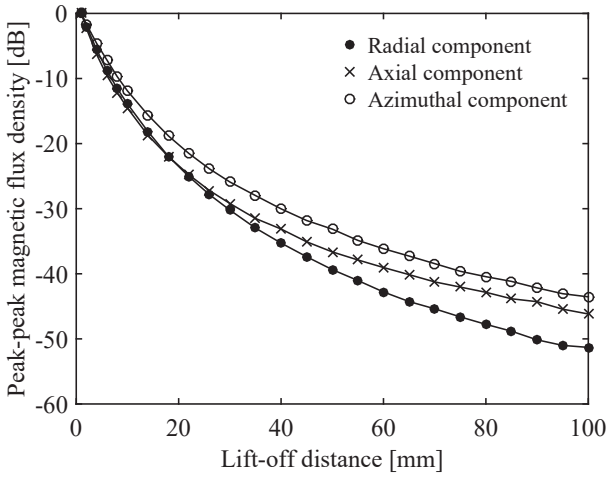

Figure 6: The peak-to-peak (as defined in Fig. 1) in the components of the magnetic flux density varying with lift-off for a diameter $3T \times 3T \times T/3$ defect depth.

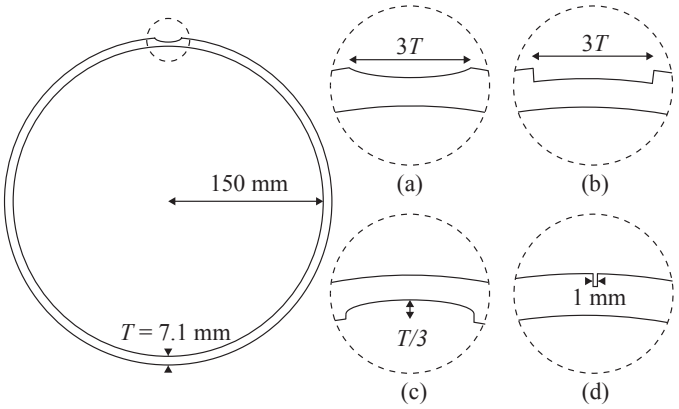

Figure 7: Cross sectional slice through the centre of the pipe showing the different defect geometries used for FE studies. (a) Outer concave defect; (b) outer circumferential slot (1 mm width); (c) inner concave defect; (d) outer axial slot ($3T$ length). Inner slots were modelled but are not pictured.

The peak-to-peak magnetic flux density falls rapidly with increasing lift-off, decreasing by 20 dB relative to the signal at the pipe surface in the first 20 mm lift-off. As the lift-off is increased further, the signal drops by a lesser extent, losing an additional 20 dB over the next 40–60 mm. As the lift-off becomes large in comparison to the defect size, the defect behaves as a magnetic dipole which loses amplitude with the cube of the lift-off distance. With 2 A current in the pipe the absolute values at the surface are 946 nT, 353 nT and 526 nT in the radial, axial and azimuthal components respectively, dropping to 46 nT, 15 nT and 31 nT at 25 mm lift-off.

4.2.2. Defect geometry study

The spatial distribution of the magnetic flux density was predicted for a number of different defect geometries and 2 A quasi-DC current in the pipe. Concave defects of maximum depth $T/3$ and diameter of $3T$ were chosen to represent corrosion patches on both the inner and the outer pipe wall. Due to the curvature of the pipe, the inner wall concave defect had a slightly larger volume in order to maintain the same curvature and and maximum depth as the outer wall concave defect. Flat bottomed slots of the same depth, a width of 1 mm and a length of $3T$ were chosen to represent cracks. The extreme cases of the slot oriented along the pipe axis and along its circumference were modelled. The defect geometries are shown schematically in Fig. 7.

The spatial distributions of the perturbation in the magnetic flux density caused by current deflection around the outer wall concave defect at a lift-off distance of 10 mm are shown in Fig. 8. The defect is centred below the origin of the diagrams. B_r exhibits a dipolar profile with peaks azimuthally separated by a distance greater than the defect width due to the clockwise and anticlockwise rotation of the current around either side of the defect. The axial component is quadripolar due to the deflection of the current direction as it avoids the defect. The spatial distributions were calculated for the other defect geometries and the peak-to-peak values of each component of $\bar{B}$ are shown in Table 2. It can be seen that when the defect is located on the outer wall, the resulting perturbation in $\bar{B}$ is larger in magnitude than for the same inner wall defect. This is largely due to the increased distance between the defect and the sensor and the reduction of leakage flux due to the presence of additional ferromagnetic steel between the inner wall defect and sensor.

The slot geometry modelled produces a smaller current deflection signal than the concave defect regardless of its orientation; however, when the slot is aligned perpendicular to the undisturbed current axis, the perturbation is much greater than when they are parallel. This is due to the circumferential slot deflecting a larger amount of current than the axial slot. The signal from the slot lying parallel to the current axis is over an order of magnitude lower than the concave defect signal when it is aligned along z, indicating the weakness of the technique in locating longitudinally oriented cracks.

Table 2: Peak-to-peak of magnetic flux density components due to current deflection around internal (I) and external (E) concave and slot defect geometries predicted 25 mm above the surface of a 6" pipe carrying 2 A current.

Defect Geometry	**I/E**	**Peak-peak [nT]**		
		$\boldsymbol{B_r}$	$\boldsymbol{B_z}$	$\boldsymbol{B_\theta}$
$3T \times 3T \times T/3$	E	45.7	14.8	30.7
$3T \times 3T \times T/3$	I	34.8	11.4	23.6
$3T \times T/3$ slot (z aligned)	E	3.9	1.3	3.1
$3T \times T/3$ slot (z aligned)	I	2.7	1.0	2.3
$3T \times T/3$ slot (θ aligned)	E	27.7	9.2	16.9
$3T \times T/3$ slot (θ aligned)	I	18.5	6.2	11.9

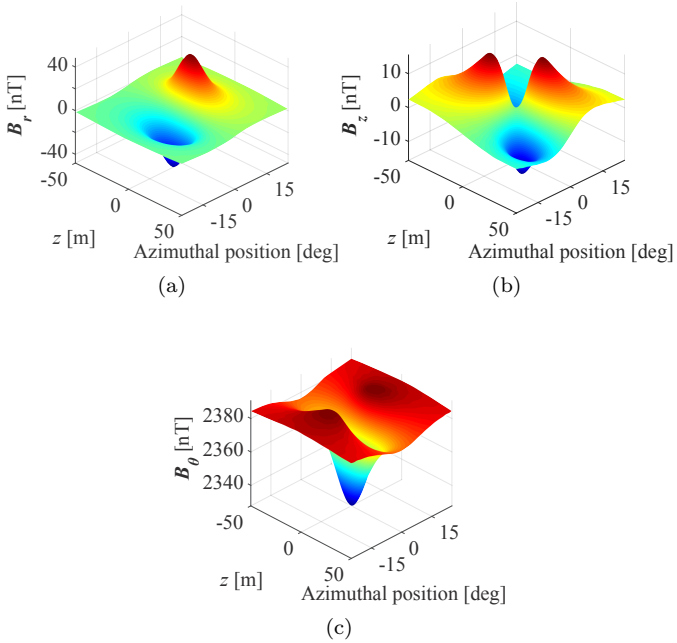

Figure 8: Spatial distributions of the (a) radial; (b) axial and (c) azimuthal components of the magnetic flux density arising from current deflection from a $3T \times 3T \times T/3$ defect 10 mm below the solution surface.

4.2.3. Pipe features and bends

Pipe features will affect the current distribution in the pipe. At a pipe bend the current will preferentially flow on the inner side of the bend as it offers the shortest path. This affects each component of the magnetic flux density profile surrounding the pipe in different ways. The majority of the current flows in the direction of the pipe axis, $\hat{z}$. As the axial component of the current density J_z is much higher on the innermost point of the bend than on the outermost point, the resulting azimuthal magnetic flux density is also much greater on the inner side of the bend. This is shown in Fig. 9 (a) at 25 mm lift-off from a 6" pipe with a bend of 60° and bend radius of 1.5× the pipe diameter, D carrying 2 A quasi-DC current.

On a uniform, defect-free section of straight pipe, the axial and radial components of the magnetic flux density are identically zero as the current density only has an axial component. However, this is no longer true for a bent pipe due to the current flowing away from the outer side of the bend. There is therefore a non-zero azimuthal component of the current density, J_θ on either side of the bend on both the top and the bottom side of the pipe. The polarity of J_z is opposite at either side of the bend as the current flows towards and away from the outer edge of bend. This current distribution results in a four-lobed axial magnetic flux density profile surrounding the pipe as illustrated in Fig. 9 (b). A perturbation in the radial component of the magnetic flux density also occurs as a magnetic flux density is induced in the direction perpendicular to the plane in which the bend lies.

It can be seen that variation in the azimuthal magnetic flux density due to the bend is much greater than that in the axial component, due to the fact that the $J_z >> J_\theta$ in the region of the bend. For this bend geometry, the peak-to-peak variation in B_θ and B_z are 2375 nT and 278 nT respectively. In the axial component, this is an order of magnitude larger than the signal from the concave or circumferential slot defects modelled in section 4.2.2, whereas in the azimuthal component the variation is three orders of magnitude greater. The peak-to-peak of the perturbation in the radial component of the magnetic flux density is 300 nT and consistently of a similar amplitude to the axial component. Various bend geometries were modelled from 5°–90° with radii of $3D$–$6D$. The peak-to-peak variation in B_r, B_z and B_θ increased for bends of smaller radius and greater angle. For the shallowest bend of 5° with a bend radius of $3D$, the perturbations in B_r, B_z and B_θ were 50 nT, 44 nT and 311 nT respectively, rising to 334 nT, 296 nT and 2604 nT for a 90 ° bend with a bend radius of $1.5D$.

There are a number of factors at a bend which affect the sensitivity of a scanning technique. Firstly, the increase in current density on the inner edge of the bend would result in current deflection signals from defects being of a higher amplitude than those located on the outer edge. This is due to the defect signal amplitude being proportional to the amplitude of current in the pipe where the defect is located. Secondly, the orientation of the sensors with the cylindrical co-ordinate system of the pipe would be more difficult to achieve over a pipe bend than when the pipe is straight. This would probably result in the large azimuthal magnetic flux density being detected by sensors intended to measure the radial and axial components of the magnetic flux density, causing large offsets that could easily exceed the amplitude of a defect signal. Finally, even if perfect orientation with the cylindrical co-ordinate system of the pipe could be maintained, the current distribution in the pipe at a bend results in non-zero axial and radial components of the magnetic flux density, so making the detection of a defect more difficult. The fact that the spatial frequency of typical defect signals is much greater than that of the perturbations in $\bar{B}$ due to the bend could be exploited to increase the sensitivity to defects. For the shallow bend of $\sim 5°$ the more slowly varying magnetic flux density from the bend is of a similar order of magnitude as typical defect signals in B_r and B_z and could possibly be corrected for, however the magnetic flux density due to sharp bends is of a much greater amplitude and could severely affect the sensitivity of a scan. Maintaining sensor alignment on a sharp bend would also be more challenging. Stationary sensors used for SHM would not be affected by these variations, although the amplitude of a current deflection signal could be increased or decreased relative to that on a straight pipe depending on where the defect was located on the bend.

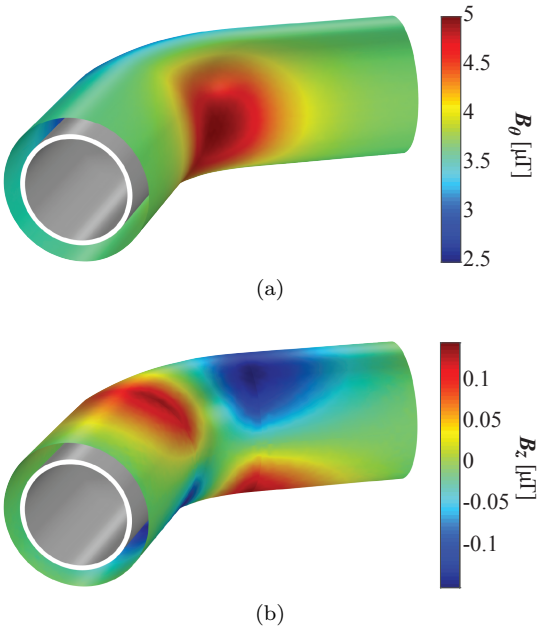

Figure 9: (a) Azimuthal and (b) axial components of $\bar{B}$ plotted on a surface at 25 mm lift off from a bent 6" schedule 40 pipe carrying 2 A quasi-DC current (bend angle: 60°, radius: 1.5×D). The unit vector $\hat{z}$ points along the pipe axis.

4.2.4. Nearby ferromagnetic objects

Phase sensitive detection is effective at suppressing spurious magnetic noise from external sources such as the mains frequency yet local variations in the spatial distribution of the magnetic flux density can be caused by factors other than current deflection from defects. Ferromagnetic objects concentrate magnetic flux, so if a ferromagnetic object such as a nail were to fall close to the scanning path of a magnetic sensor array, a local variation in the magnetic flux density would be observed as the sensors move past the object. There is a possibility that this local variation in the magnetic flux density could be interpreted as a current deflection signal caused by a defect leading to an increased false call rate of the technique. This has prompted an FE study to investigate how the presence of a ferromagnetic object external to the pipe affects the sensitivity of the technique.

Two cube sizes of side length 10 mm and 25 mm were modelled. The relative permeability of the cube was set to $\mu_r = 100$ (approximately representing a carbon steel), and the block was positioned at a varying distance between 22–150 mm from the pipe surface. The solution surface representing the sensor location was positioned at 10 mm or 25 mm lift-off as shown schematically in Fig. 10 (a). The peak-to-peak of the radial and axial components of the magnetic flux density were found on this surface for each combination of size of the block and distance from the pipe. The resulting curves are shown in Fig. 10 for the solution surface at a lift-off distance of 10 mm (b) and for a lift-off of 25 mm (c). On these curves, there is an overlay of the peak-to-peak values resulting from deflection of a 2 A current around a $3T \times 3T \times T/3$ defect positioned in the pipe outer surface, as calculated in the previous FE study from section 4.2.2.

Table 3 shows the minimum distance between the block and the solution surface for the peak-to-peak signal caused by flux concentration from the ferromagnetic block to be equal in amplitude or smaller than the concave defect. These results represent the case where the block falls exactly in line with the sensor in the axial and circumferential directions so the distance vector separating the two is purely radial. When the lift-off is 25 mm and if the ferromagnetic block is located closer than 71 mm radially (in the case of a 25 mm side length cube), this could result in an equal amplitude perturbation as a $3T \times 3T \times T/3$ defect when considering the radial component of $\bar{B}$. Interestingly, the perturbation of the magnetic flux density by the block affects the axial component less strongly, and it only exceeds the defect signal magnitude when the block is positioned less than 48 mm radially from the pipe surface.

When the sensor is positioned at 25 mm lift-off, the measured perturbation from current deflection in the pipe due to the presence of defects will be smaller than when the measurement is taken at 10 mm lift-off. This results in the higher lift-off measurements being more susceptible to false calls from the presence of an external ferromagnetic object, as it will match the defect signal amplitude at a greater radial separation than if the sensor were closer to the pipe. For example in this case of the 25 mm block, the minimum separation distance between the block and sensor for the block perturbation to match the peak-to-peak defect amplitude in B_r is 22 mm at 10 mm lift-off in comparison to 49 mm at 25 mm lift-off.

Table 3: Comparison of the radial separation between a $\mu_r = 100$ block and a sensor aligned axially and circumferentially with the block for which the resulting perturbation in magnetic flux density profile is of equal magnitude as a $3T \times 3T \times T/3$ concave defect located in the outer surface of the pipe.

Block side length [mm]	**Lift-off [mm]**	**Radial separation at which block signal amplitude matches $3T \times 3T \times T/3$ pk-pk signal [mm]**	
		for B_r	**for B_z**
10	10	18	13
25	10	32	27
10	25	67	29
25	25	71	48

The data in Fig. 10 and Table 3 represent the worst case scenario where the location of the peaks in the spatial distribution of the magnetic flux density caused by the steel block fall on the same radial line as the sensor. In order to further evaluate the amount by which the block can disturb a defect signal, the angular extent over which the perturbation caused by the block is greater than the defect signal was computed. The results are shown in Fig.

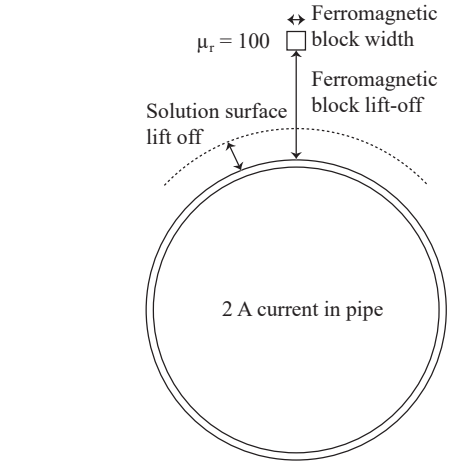

(a)

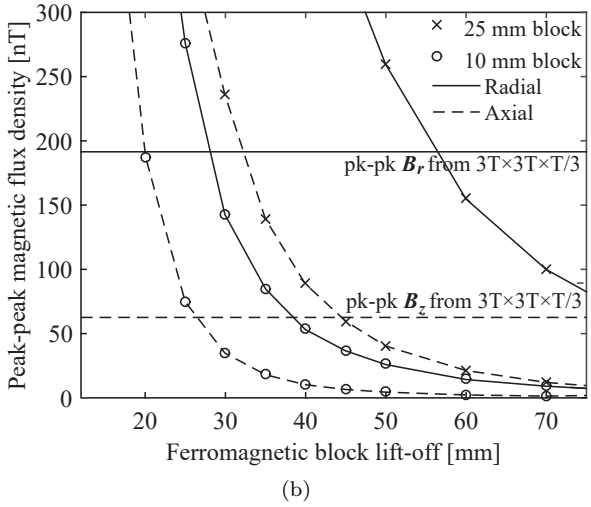

(b)

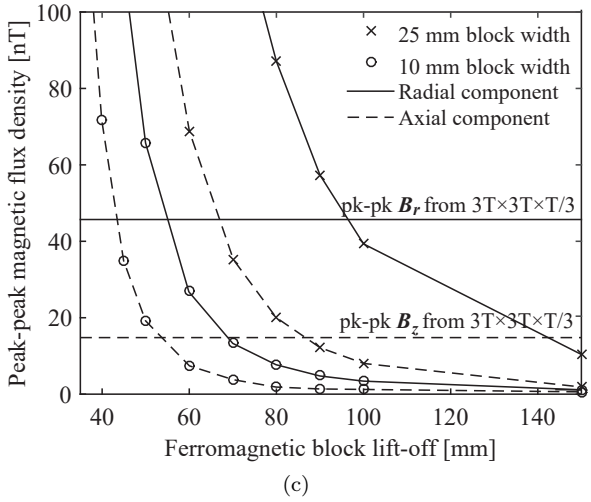

(c)

Figure 10: (a) Schematic of model geometry. Peak to peak of magnetic perturbations at (b) 10 mm and (c) 25 mm from a uniform pipe carrying 2 A current when a ferromagnetic ($\mu_r = 100$) 10 mm side length or 25 mm side length block is located at a varying distance from the pipe. The peak-to-peak values of B_r and B_z from a $3T \times 3T \times T/3$ outer wall defect at the same lift-off plotted for comparison. Points joined with straight lines to ease visualisation.

11 (a) and (b). To calculate these curves, the block was positioned axially in line with the sensor, and the angular extent over which the absolute values of B_r and B_z exceeded those of the concave defect were calculated as the distance between the block and pipe was increased.

These curves show that when the sensor is positioned at a higher lift-off, the perturbation from the steel cube is greater than the defect signal over a larger angular range than when the sensor is positioned closer to the pipe. Clearly, the larger cube is more detrimental to the signal than the smaller cube. In the worst case scenario modelled, the sensor is at 25 mm lift-off and the block is positioned 5 mm further from the pipe than the sensor. Here, there is an angular range of 58° over the circumference where the block perturbation is greater than the defect signal in B_r. For the 10 mm side length block at the same distance, the angular range that exceeds the defect signal falls to 36° in the radial component and 24° in the axial component.

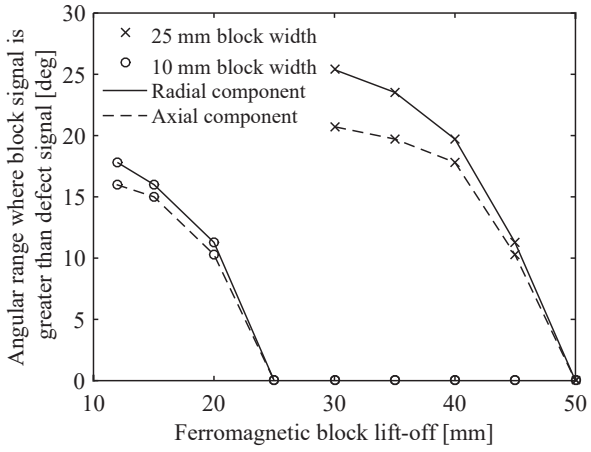

(a)

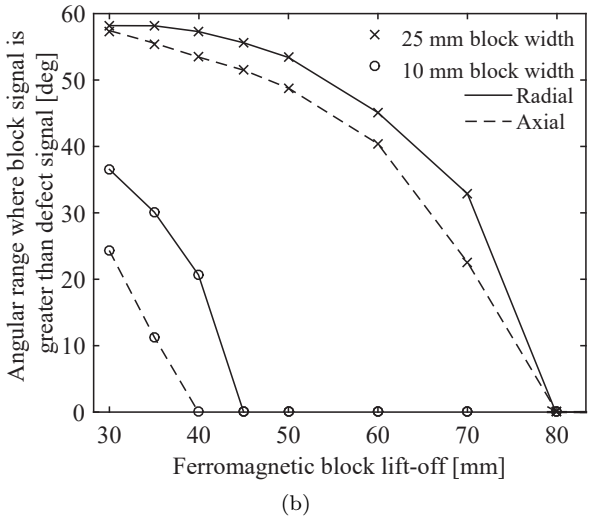

(b)

Figure 11: The angular range over which the perturbation caused by an outer wall $3T \times 3T \times T/3$ defect is exceeded by the presence of a 10 mm or 25 mm side length steel cube at various radial distances from a sensor positioned at (a) 10 mm lift-off and (b) 25 mm lift-off. Points joined with straight lines to ease visualisation.

4.3. Magnetic measurements of current deflection from defects

Measurements of current deflection from flat bottomed slots milled into the outer surface of a 1.5 m long six inch schedule-40 austenitic steel pipe were taken in order to validate the FE model and determine the performance of an experimental measurement of current deflection. The austenitic pipe scanned had three external flat bottomed slots with maximum depths of $\frac{T}{4}$, $\frac{T}{2}$ and $\frac{3\times T}{4}$ respectively. The $\frac{T}{2}$ slot was positioned half way along the pipe, and the remaining slots were located 0.4 m from either end and circumferentially separated by 120° in order to minimise the interaction between the signals. A measurement of each component of the magnetic flux density was taken every 15 mm over a length of 1.1 m and around the entire circumference at every 10°. Each sensor was averaged for 25 seconds and the current frequency was 25 Hz (resulting in a skin depth of ∼83 mm) which is low enough to ensure quasi-DC operation in non-magnetic austenitic steel. The magnetic flux density profiles in a section of the scan around the deepest defect are shown in Fig. 12 (a)-(c). The data was cubically interpolated to a finer spatial resolution of every 1° and every 2.5 mm. The characteristic perturbations of current deflection are exhibited in these measurements, as in the FE predictions in Fig. 8. It can be seen in Fig. 12 (c) that there is some asymmetry about the defect centre in the azimuthal direction. This is due to changes from the uniform pipe geometry due to manufacturing tolerances in the wall thickness.

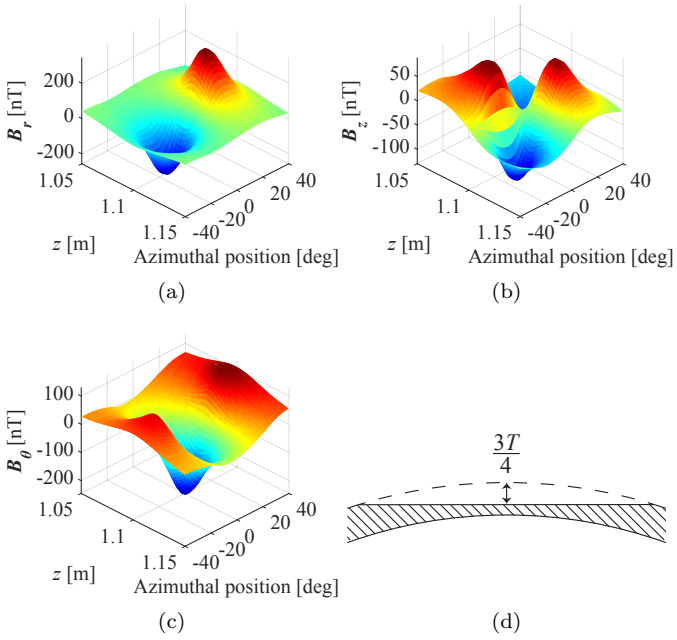

Figure 12: Spatial distributions of the (a) radial; (b) axial and (c) azimuthal components of the magnetic flux density arising from current deflection from a flat bottomed slot (shown schematically in (d)) measured at 10 mm lift-off from the pipe.

A circumferential scan centred above the deepest slot taken at 10 mm lift-off was compared to the identical defect geometry recreated in FE. In order to correct for the slight variations in wall thickness caused by manufacturing tolerances, the baseline was established by taking an additional circumferential scan offset axially by a distance of 50 mm where the defect signal is diminished but the perturbations in B_r caused by the nominal wall thickness changes (which vary slowly along the pipe axis) remain. The measurement of B_r over the circumferential scan is plotted in comparison to the FE prediction in Fig. 13. The FE data is plotted as a dashed line. There is an excellent agreement between the baseline corrected scan and the FE data, both exhibiting peak-to-peak amplitudes of 605 nT.

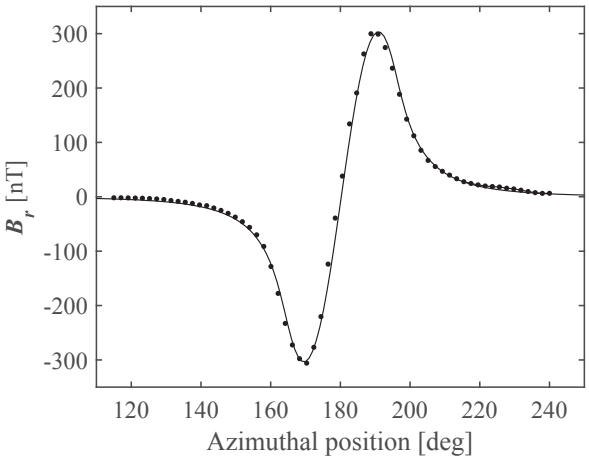

Figure 13: Comparison of FE prediction (solid line) with a circumferential scan (dots) of the radial component of the magnetic flux density at 10 mm lift-off.

4.4. Measurements performed on a seamless carbon steel pipe

The previous current deflection measurements were carried out on an austenitic stainless steel pipe. As the pipe was non-magnetic, a relatively high current frequency could be permitted before the skin effect changed the current distribution inside the pipe wall. As the majority of pipeline is manufactured from ferromagnetic carbon steel, it is important that the technique also functions on such materials. Scans of the magnetic flux density surrounding a 1.5 m length of six inch schedule 40 carbon steel pipe were taken. The pipe was manufactured under the ASTM A106B specification for seamless carbon steel pipe for high-temperature service which permits a wall thickness variation of 12.5% from the nominal wall thickness of 7.11 mm and an outer diameter variation of +1.6/-0.8 mm [46].

An ultrasonic EMAT scanning system (Innerspec Powerbox H) was used to obtain a wall thickness map of the pipe. The system consists of a rotary encoded EMAT transducer operating at 50 kHz and driven at 1200 V. The encoder allowed B-scans to be performed along the pipe axis with a spatial resolution of 5 mm. A laser guide was used to

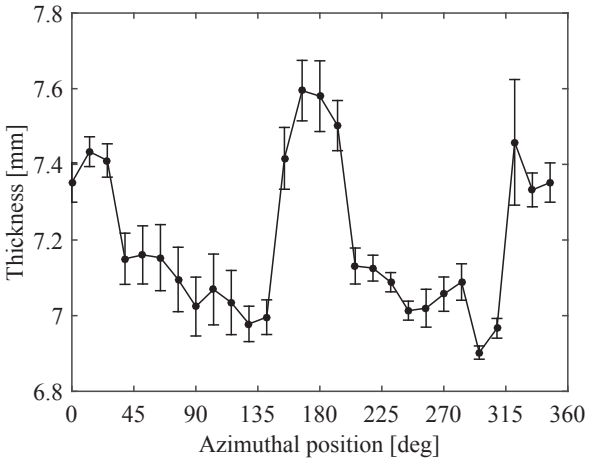

Figure 14: Profile of the mean wall thickness measured along a 1.5 m section of pipe as a function of circumfrential position. Error bars show the standard deviation.

help ensure that all scans were performed parallel to the pipe axis. After each scan, the pipe was rotated by 20 mm (13.5°) before another scan was completed until the entire surface of the pipe had been measured. The average thickness was measured as 7.14 mm with a maximum of 7.72 mm and a minimum of 6.81 mm. These fall within the specified tolerances. A strong variation in wall thickness was noted around the circumference of the pipe. The average standard deviation of the wall thickness around the circumference was 0.20 mm, whereas the average standard deviation of a 1.5 m scan along the axis of the pipe was just 0.02 mm. The mean and standard deviation of the thickness measured along the pipe axis is shown in Fig. 14.

The magnetic flux density surrounding the pipe was mapped at lift-off distances of 10 mm and 50 mm with a current frequency of 5 Hz and 25 Hz. The results from the 50 mm lift-off scan are shown in Fig. 15. The figures exhibit a periodic helical variation in $\bar{B}$ most clearly seen in the axial component (a). The cause of this helical perturbation is the material property changes that accompany the seamless pipe manufacture process [47]. The helical profile in the magnetic field surrounding seamless pipes has been referred to as "seamless pipe noise" (SPN) in reference to the MFL testing of seamless pipelines, where flux leakage from defects can easily be hidden leading to an increased number missed defects when pigging [48]. A number of different algorithms have been proposed in order to correct for the periodic noise and considerably improve the detectability of defect signals [48, 49, 50].

In addition to the SPN, there are also regions of increased intensity along the pipe axis centred around 0° and 180° in the radial and azimuthal components of $\bar{B}$ in Fig. 15 that can be attributed to the regions of increased wall thickness shown in Fig. 14. The low standard deviation in thickness along the pipe axis corroborates the fact that the high intensity region is not present in B_r as the axially flowing current cannot be perturbed much in the azimuthal direction by variations in the wall thickness.

The peak-to-peak of the variations in $\bar{B}$ from the SPN are of the same order of magnitude as the current deflection signals resulting from a $3T \times 3T \times T/3$ outer wall defect, therefore it is important that the noise can be suppressed if the technique is to be applied successfully to the scanning of seamless pipes. The application of SPN correction algorithms and subsequent baseline subtraction is a possible method to increase the signal to noise ratio.

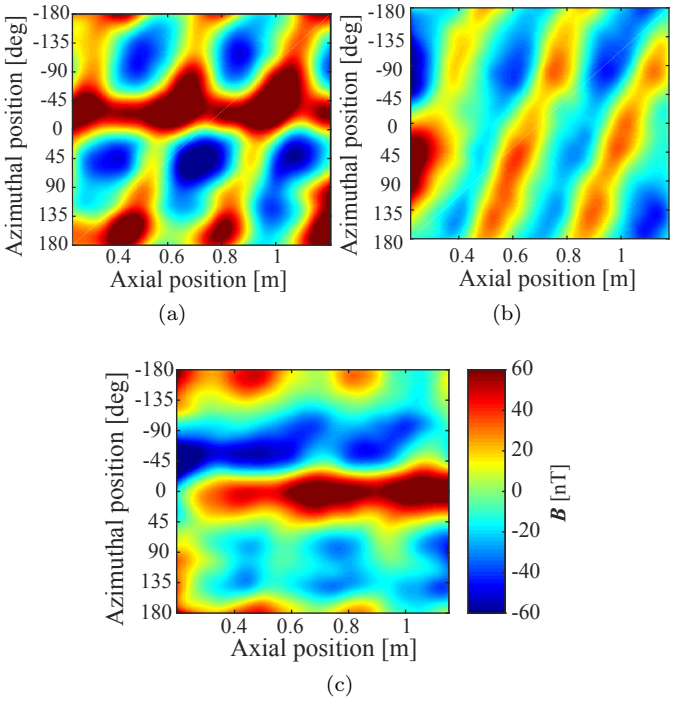

Figure 15: Spatial distributions of the (a) radial; (b) axial and (c) azimuthal components of the magnetic flux density measured at 50 mm lift-off from a defect free seamless carbon steel pipe carrying 2 A, 5 Hz current. All figures use the same scale.

5. Discussion

5.1. Industrial application for defect screening by scanning

5.1.1. Detectability of defect signals and scanning speed

From scans of the magnetic flux density surrounding a defect-free welded carbon steel pipe carrying 2 A quasi-DC current, the axial and radial components remained close to zero with standard deviations of a few hundred pT. FE predictions of the peak-to-peak perturbations in $\bar{B}$ caused by current deflection around a $3T \times 3T \times T/3$ defect were at least two orders of magnitude greater than this at a distance of 25 mm from the pipe surface. The current deflection signal amplitude is proportional to the amount of current injected, so a larger lift-off could be tolerated if the current amplitude were increased. One must note,

however, that at an increased lift-off the spatial resolution of the defect signals and the efficiency of background suppression by gradiometry are both reduced.

FE simulations showed that the signal from a slot aligned with the pipe axis was an order of magnitude lower than one aligned circumferentially. This implies that current deflection could be an effective tool to screen for pipe corrosion on both the inner and outer wall, however it should be used in conjunction with alternative techniques if the detection of longitudinal cracks is a requirement. The amplitude of the signals predicted from the modelled defects at 25 mm lift-off falls within the sensitivity range of inexpensive commercially available MR sensors [42]. The sensors could be employed to measure current deflection signals via an external pipe crawler, or possibly a subsea ROV for pipelines, to screen for defects at tens of mm lift-off from the pipe. The use of magnetic sensors outside pipe insulation and cladding is attractive as its removal is time consuming and expensive, although the use of ferromagnetic cladding could reduce the sensitivity of the technique. There must be a point of contact to the pipe for the injection and retrieval of current, although coating removal may often be avoidable by utilising exposed sections with electrical contact to the pipe such as valves. Where coating removal is unavoidable, a single point of contact for the current injection would suffice so long as enough distance is left for the current distribution to become uniform around the circumference of the pipe before measurements are to be taken. The current injection points may also be a very long distance (∼kilometres) apart whereas guided wave inspection is typically limited to a maximum of 100 m range and less in buried pipes or those with lossy coatings

Phase sensitive detection has been used to eliminate spurious magnetic noise sources such as the geomagnetic field, dynamic fields from moving magnetic objects and the signal associated with the mains frequency. This is achieved by using the current in the pipe as a reference signal, however in order to achieve sensitivity of both inner and outer wall defects, the current distribution must not be limited by the electromagnetic skin effect. When testing ferromagnetic carbon steel pipes, this limits the frequency to a maximum of ∼10 Hz for a six-inch schedule 40 pipe and even lower for pipes of greater wall thickness. Non-magnetic austenitic steel pipes can use a much higher frequency of the order of kHz. The low frequency condition demands that the sensors be stationary during acquisition, which may take several seconds. This places limits on the overall scanning speed of carbon steel pipes.

5.1.2. Potential issues affecting sensitivity

A bend in the pipe could greatly affect the sensitivity of the technique in scanning mode. The reduction in current density at the outer edge of the pipe would reduce the amplitude of defects located there. In addition, the current distribution at a bend results in non-zero distributions of the radial and axial components in the magnetic flux density surrounding the bend which would are likely difficult to suppress using gradiometric sensing (using multiple sensors separated by an axial distance in order to remove a slowly varying background signal while retaining the defect signal).

External ferromagnetic objects may be present along the scanning path of the magnetic sensors, so FE modelling was used to reveal the likelihood of this resulting in a false call. This study revealed that sensitivity is more readily affected by the presence of an external ferromagnetic object if the sensor lift-off is higher. The results suggest that the scanning path should be free from ferromagnetic objects positioned closer than ∼25-100 mm to the sensor (depending on the lift-off and object size) if the false call rate is to be minimised. The sensitivity is also likely to be affected by the presence of pipe supports.

Ultrasonic thickness measurements of defect free seamless pipe revealed a low deviation from the nominal wall thickness along the pipe axis relative to the thickness variation around the circumference. This suggests that gradiometric sensing with axially spaced sensors could be effective in increasing the sensitivity by suppressing the signal resulting from the wall thickness varying within manufacturing tolerances. Indeed, by using a baseline acquired at an axial distance of 50 mm from a circumferential scan around a flat bottomed slot, good agreement between experiment and FE was obtained.

Magnetic measurements of seamless pipes detected spatially periodic noise which has the potential to mask current deflection signals measured during a scan as the peak-to-peak amplitude of the noise was of a similar magnitude to the expected defect signal. To maximise the sensitivity to defects on seamless pipe, algorithms to correct for this noise such as those used in MFL testing should be employed. Due to phase-sensitive detection, the technique is not sensitive to the DC magnetisation in the pipe that may be present from previous MFL testing; however, a sufficiently low current frequency should be employed in these circumstances such that the current distribution is not limited by magnetic variations and is only affected by the geometry of the pipe.

The central rod used for the current return path in the lab experiments would not be available to suppress the azimuthal component of $\bar{B}$ if implementing current injection in an industrial setting; therefore it is suggested that tri-axial sensors would be used to monitor all orthogonal components of the flux density and only the radial and axial components be used for defect detection. The presence of the large azimuthal field component could result in an offset in the measured $\bar{B}$ from the radial and axial sensors if alignment with the cylindrical co-ordinate system of the pipe were not maintained. Measuring the inclination of the sensors during the scan would probably be a requirement to correct for any misalignment.

5.2. Industrial application in structural health monitoring

An additional attractive use of current deflection is to monitor the growth of existing defects or the formation of

defects at hotspots by the permanent installation of magnetic sensors outside the pipe. In order to maximize the sensitivity for SHM, temporal baseline subtraction is utilized. A sensor is interrogated at regular time intervals and the initial signal is subtracted from subsequent readings. If the residual is zero then there is no change in the metal geometry. If the residual is non zero after a reading, this can be attributed to the growth or appearance of a defect. During a stability measurement using an AMR sensor at a fixed position, the magnetic flux density remained close to zero with a standard deviation of a few hundred pT, suggesting the growth of a defect resulting in a magnetic signal that exceeds this threshold could be detected. If AMR sensors were permanently installed in the field, a long averaging time and temperature correction should be used to increase the sensitivity. The products of corrosion are non-conducting but highly magnetic, therefore further research is required to investigate the influence of the magnetic property changes accompanying corrosion to the sensitivity of the technique.

The reduction in current density at the outer edge of a bend would reduce the defect signal amplitude somewhat, although an increased current could make up for the loss in sensitivity. Spatial distributions in the magnetic flux density that would affect the sensitivity of the technique in scanning mode (such as SPN and slight deviations of the pipe from the nominal wall thickness and outer diameter) do not change over time, and would not impact the sensitivity of a SHM technique provided the sensors remain at a fixed position. If the position or orientation of the sensor changes (e.g. due to an impact), the measured magnetic flux density would also change. Maintaining and accounting for changes in the sensor orientation will therefore be crucial to the success of an SHM technique based on current deflection.

6. Conclusion

In this paper, the potential for using quasi-DC current deflection to detect and monitor defects at a significant lift-off from a pipe using magnetic sensors has been discussed. A flexible FE model has been validated using circumferential scans of induced magnetic flux density from current deflection around a flat bottomed slot. The model was used to determine the rate of decay of a defect signal amplitude with lift-off. It also enabled prediction of current deflection signals from various defect geometries, and the effect of external ferromagnetic objects and pipe bends on the sensitivity. Experimental measurements of the induced magnetic flux density from a current carrying pipe suggest that the threshold for defect detection is of the order of tens to hundreds of pT when used as either a NDT or SHM technique. A threshold at this level suggests that typical corrosion-like defects could be detectable using MR sensors at around 50 mm lift-off when the pipe carries a few amps of current ($\sim$500 A/m^2 cross sectional area). There is a possibility of galvanic injection using the cathodic protection testing post infrastructure that exists on many pipelines. There is potential to apply the technique to the inspection or monitoring of pipework without the need to remove the insulation or (non-ferromagnetic) cladding.

The slowly varying pipe wall thickness in the axial direction could be exploited to maximise the sensitivity of the technique when implemented in the scanning regime by using baseline subtraction from measurements taken along the same axial scan line. As a screening method, the technique could be implemented using an external pipe crawler. If using the technique for SHM, factors that result in spatial variations in the magnetic flux density (such as material property variations and deviations from the nominal pipe wall due to manufacturing tolerances) will not affect the sensitivity provided the magnetic sensors remain stationary. The presence of nearby ferromagnetic objects is also not an issue for SHM provided they do not move. As an SHM method, the technique could be attractive for monitoring the growth of defects at hotspots, corrosion under insulation on pipework, or at pipeline features to which ILI methods are blind.

Acknowledgements

The authors would like to acknowledge funding provided by EPSRC grant EP/I017704/1 for the Centre for Doctoral Training in NDE and by project partner BP plc. for the support of this research.

7. References

[1] H. A. Kishawy, H. A. Gabbar, Review of pipeline integrity management practices, International Journal of Pressure Vessels and Piping 87 (7) (2010) 373–380.

[2] J. Quarini, S. Shire, A Review of Fluid-Driven Pipeline Pigs and their Applications, in: Institution of Mechanical Engineers, Part E: Journal of Process Mechanical Engineering, Vol. 221, 2007, pp. 1–10.

[3] S. Safizadeh, M. Hasanian, Gas Pipeline Corrosion Mapping Using Pulsed Eddy Current Technique, International Journal of Advanced Design and Manufacturing Technology 5 (1) (2011) 11–19.

[4] W. Cheng, Pulsed Eddy Current Testing of Carbon Steel Pipe Wall-thinning Through Insulation and Cladding, Journal of Nondestructive Evaluation 31 (3) (2012) 215–224.

[5] I. Silva, Y. Santos, L. Batista, C. Farias, Corrosion Inspection Using Pulsed Eddy Current, in: 11th European Conference on Non-Destructive Testing, Prague, 2014, p. 8.

[6] Y. Li, B. Yan, D. Li, Y. Li, D. Zhou, Gradient-field pulsed eddy current probes for imaging of hidden corrosion in conductive structures, Sensors and Actuators A: Physical 238 (2016) 251–265.

[7] J. de Raad, T. Bouma, A. Bonisch, Rapid corrosion screening in up to 30 mm wall thickness for plates and pipe, Insight 44 (2) (2002) 97–103.

[8] Innospection, SLOFEC Technique for Pipe Scanning (2015). URL `http://www.innospection.com/pdfs/SLOFECPipeScanning.pdf`

[9] Dooson Babcock Energy Ltd., Evaluation of the effectiveness of non-destructive testing screening methods for in-service inspection, Tech. rep. (2009).

[10] J. W. Wilson, G. Y. Tian, Pulsed electromagnetic methods for defect detection and characterisation, NDT & E International 40 (4) (2007) 275–283. doi:10.1016/j.ndteint.2006.12.008.
[11] K. R. Larsen, Dynamic pulsed eddy current inline inspection technology assesses unpiggable pipelines, Materials Performance 54 (4) (2015) 14–16.
[12] G. L. Burkhardt, T. H. Goyen, A. J. Parvin, R. H. Peterson, R. F. Tennis, Small Diameter Remote Field Eddy Current Inspection for Unpiggable Pipelines, in: ASME International Pipeline Conference, Vol. 2, American Society of Mechanical Engineers, Calgary, Canada, 2008, pp. 41–44.
[13] P. Laursen, D. D'Zurko, G. Vradis, C. Swiech, Robotic Inspection of Unpiggable Natural Gas Transmission and Distribution Pipeline, in: 8th International Pipeline Conference, ASME, Calgary, Canada, 2010, pp. 407–410.
[14] M. Lowe, D. Alleyne, P. Cawley, Defect detection in pipes using guided waves, Ultrasonics 36 (1-5) (1998) 147–154.
[15] P. Cawley, M. J. S. Lowe, D. N. Alleyne, B. Pavlakovic, P. D. Wilcox, Practical long range guided wave testing: applications to pipes and rail, Materials Evaluation 61 (1) (2003) 66–74.
[16] D. Alleyne, B. Pavlakovic, M. Lowe, P. Cawley, Rapid, Long Range Inspection of Chemical Plant Pipework Using Guided Waves, Key Engineering Materials 270-273 (2004) 434–441.
[17] E. Leinov, M. J. Lowe, P. Cawley, Ultrasonic isolation of buried pipes, Journal of Sound and Vibration 363 (2016) 225–239.
[18] F. Honarvar, F. Salehi, V. Safavi, A. Mokhtari, A. N. Sinclair, Ultrasonic monitoring of erosion/corrosion thinning rates in industrial piping systems., Ultrasonics 53 (7) (2013) 1251–8.
[19] K. Edalati, N. Rastkhah, A. Kermani, M. Seiedi, A. Movafeghi, The use of radiography for thickness measurement and corrosion monitoring in pipes, International Journal of Pressure Vessels and Piping 83 (10) (2006) 736–741.
[20] EN 16407 Parts 1 and 2: Newly published European standards for the in-service digital and film radiography of pipes.
[21] J. Guo, L. Zeng, B. Liu, High-quality image reconstruction from exterior helical cone-beam CT data for NDE of industrial pipelines, Insight - Non-Destructive Testing and Condition Monitoring 53 (10) (2011) 534–541.
[22] P. S. Ong, V. Patel, A. Balasubramanyan, Quantitative characterization of corrosion under insulation, Journal of Nondestructive Evaluation 16 (3) (1997) 135–146.
[23] U. Ewert, M. Tschaikner, S. Hohendorf, C. Bellon, M. I. Haith, P. Huthwaite, M. J. Lowe, Corrosion Monitoring with Tangential Radiography and Limited View Computed Tomography (To be published), in: Review of Progress in Quantitative Nondestructive Evaluation, Baltimore, 2014.
[24] U. Zscherpel, U. Ewert, S. Infanzon, N. Rastkhan, P. R. Vaidya, I. Einav, S. Ekinci, Radiographic Evaluation of Corrosion and Deposits in Pipelines: Results of an IAEA Co-ordinated Research Program, in: European Conference on NDT, Berlin, 2006.
[25] D. C. Jiles, Theory of the magnetomechanical effect, Journal of Physics D: Applied Physics 32 (1999) 1945–1945.
[26] I. Kolesnikov, Magnetic Tomography Method (MTM): A Remote Non-destructive Inspection Technology for Buried and Sub Sea Pipelines, in: OTC Arctic Technology Conference, Offshore Technology Conference, 2014.
URL https://www.onepetro.org/conference-paper/OTC-24569-MS
[27] C. Li, C. Chen, K. Liao, A quantitative study of signal characteristics of non-contact pipeline magnetic testing, Insight 57 (6) (2015) 324–330.
[28] S. G. H. Staples, C. Vo, D. M. J. Cowell, S. Freear, C. Ives, B. T. H. Varcoe, Solving the inverse problem of magnetisation–stress resolution, Journal of Applied Physics 13 (2013) 9.
[29] M. Augustyniak, Z. Usarek, Discussion of Derivability of Local Residual Stress Level from Magnetic Stray Field Measurement, Journal of Nondestructive Evaluation 34 (3) (2015) 21.
[30] G. S. Krivoi, NoPig: An above-ground inspection technique for non-piggable pipelines, Oil Gas European Magazine 34 (03) (2008) 122–124.
[31] G. G. J. Achterbosch, M. Broderick, NoPig - A New Technique in Pipeline Integrity, in: 22nd World Gas Conference, Tokyo, 2003.
[32] J. R. Singer, G. Stevick, D. King, Detecting and Monitoring Corrosion under Insulation in Piping, Mat. Corr. 52 (10) (2013) 8–10.
[33] M. C. Lugg, The First 20 Years of the AC field Measurement Technique, in: 18th World Conference on Nondestructive Testing, no. April, Durban, South Africa, 2012, p. 7.
[34] A. M. Lewis, D. H. Michael, M. C. Lugg, R. Collins, Thin-skin electromagnetic fields around surface-breaking cracks in metals, Journal of Applied Physics 64 (8) (1988) 3777.
[35] R. LeTessier, R. Coade, B. Geneve, Sizing of cracks using the alternating current field measurement technique, International Journal of Pressure Vessels and Piping 79 (8-10) (2002) 549–554.
[36] P. B. Nagy, Electromagnetic Nondestructive Evaluation, in: T. Kundu (Ed.), Ultrasonic and Electromagnetic NDE for Structure and Material Characterization: Engineering and Biomedical Applications, 1st Edition, CRC Press, Boca Raton, FL, 2012, Ch. 3, p. 890.
[37] G. Sposito, P. Cawley, P. B. Nagy, Potential drop mapping for the monitoring of corrosion or erosion, NDT and E International 43 (5) (2010) 394–402.
[38] K. Wold, G. Sirnes, Fsm Technology - 16 Years Of Field History-Experience, Status And Further Developments. (Jan 2007).
[39] F. Gan, G. Tian, Z. Wan, J. Liao, W. Li, Investigation of pitting corrosion monitoring using field signature method, Measurement 82 (2016) 46–54.
[40] R. L. Bianchetti, Galvanic Anode Installation Details, in: A. W. Peabody (Ed.), Control of Pipeline Corrosion, 2nd Edition, NACE Press, Houston, Texas, 2001, Ch. 9, p. 197.
[41] H. A. Wheeler, Formulas for the Skin Effect, Proceedings of the IRE 30 (9) (1942) 299–311.
[42] J. Lenz, S. Edelstein, Magnetic Sensors and their Applications, IEEE Sensors Journal 6 (3) (2006) 631–649.
[43] R. W. Schneider, C. H. Smith, Low Magnetic Field Sensing with GMR Sensors, Part 2: GMR Sensors and Their Applications — Sensors (1999).
[44] D. G. Altman, J. M. Bland, Standard deviations and standard errors., BMJ (Clinical research ed.) 331 (7521) (2005) 903.
[45] COMSOL, COMSOL Multiphysics (2015).
URL http://www.uk.comsol.com/
[46] ASTM A106 / A106M - 14 Standard Specification for Seamless Carbon Steel Pipe for High-Temperature Service (2014).
[47] S. Willcock, B. Tanner, P. Mundell, The magnetic properties of seamless steel pipe, Journal of Magnetism and Magnetic Materials 66 (1) (1987) 153–157.
[48] W. Han, A new denoising algorithm for MFL data obtained from seamless pipeline inspection, Russian Journal of Nondestructive Testing 44 (3) (2008) 184–195.
[49] M. Afzal, R. Polikar, L. Udpa, S. Udpa, Adaptive noise cancellation schemes for magnetic flux leakage signals obtained from gas pipeline inspection, in: 2001 IEEE International Conference on Acoustics, Speech, and Signal Processing. Proceedings (Cat. No.01CH37221), Vol. 5, IEEE, 2001, pp. 3389–3392.
[50] M. Afzal, S. Udpa, Advanced signal processing of magnetic flux leakage data obtained from seamless gas pipeline, NDT & E International 35 (7) (2002) 449–457.